RSC Advances

PAPER

Cite this: *RSC Adv.*, 2016, **6**, 73186

Influence of morphological and chemical features of biochar on hydrogen peroxide activation: implications on sulfamethazine degradation

Danlian Huang,*[ab] Yang Wang,[ab] Chen Zhang,[ab] Guangming Zeng,[ab] Cui Lai,[ab] Jia Wan,[ab] Lei Qin[ab] and Yalan Zeng[ab]

Received 7th May 2016
Accepted 27th July 2016

DOI: 10.1039/c6ra11850j

www.rsc.org/advances

This paper investigated how morphological and chemical features of biochars influenced hydroxyl radical (˙OH) generation and sulfamethazine (SMT) degradation in the presence of hydrogen peroxide (H_2O_2). Effects of SMT adsorption on H_2O_2 activation by biochar were also studied. In this study, a series of wheat chars were pyrolyzed anaerobically at six heat treatment temperatures (HTT) (300, 400, 500, 600, 700, and 800 °C) and characterized for morphological and chemical features. Higher-temperature biochar led to the higher yield of ˙OH formed during H_2O_2 activation, which might be due to the better morphological features and higher content of basic character biochar obtained at high temperature. The degradation efficiency of SMT (13.7 μM) went up from 93.4% to 100% and the pseudo-first-order rate constant increased from 0.0211 min^{-1} to 0.427 min^{-1} with the increase of charring temperature in H_2O_2/biochar system. Furthermore, biochars' reactivity toward H_2O_2 was inhibited by the adsorption of SMT on their surface. The present findings highlighted the influence of morphological and chemical features of biochar on H_2O_2 activation, and provided a new approach for biochar application to organic contaminant removal.

1. Introduction

Biochar, a fascinating carbon-rich material obtained under low oxygen conditions, has been recognized as a highly efficient adsorbent due to its large surface area, complex porosity and variable surface composition.[1–6] Compared with the studies focused on biochar for contaminant absorption, few publications have explored the performance of biochar on organic contaminants degradation, which would provide a broad application prospect for contaminant removal.

Porous carbon materials (activated carbons, carbon nanofibers, and graphite, *etc.*) were used in catalysis either as catalysts or supports, and activation of hydrogen peroxide (H_2O_2) by activated carbon has been successfully applied to the degradation of dissolved organic pollutants.[7–10] Considering the relatively low-cost and similar characteristics of biochar as that of activated carbon, the potentiality of the catalytic activity of biochar toward oxidants (H_2O_2, persulfate, *etc.*) has been extensively investigated in several literatures.[11–13] Biochar supported nanoscale zerovalent iron was successfully used in catalysis for persulfate activation, promoting the generation of sulfate radicals ($^{\cdot}SO_4^-$) and the degradation of trichloroethylene.[13] Previous reports indicated that biochars, with the redox activity and electron shuttling capacity, may be characterized as an electron shuttle for environmental remediation by directly mediating electron transfer processes and then influenced pollutant transformation reactions.[14,15] It has been found that the chars (produced from pine needles, wheat, and maize straw) showed a great performance on H_2O_2 activation, resulting in the generation of hydroxyl radicals (˙OH) and the degradation for 2-chlorobiphenyl completely.[11]

H_2O_2 and its final products are eco-friendly during the process of activation.[16,17] Additionally, the generation of ˙OH radicals was recognized as the key in chemical oxidizing of organic pollutants in H_2O_2 activation.[18,19] Therefore, it was pressed to define the influencing factors in H_2O_2 activation by biochar to improve the formation of ˙OH. The H_2O_2 activation was expected to be initiated on the surface of the char similar to the process of adsorption. While the significant effects of morphological and chemical features on the adsorption behavior of chars have been reported systematically, few studies have been done for understanding how these characteristics of biochar (surface area, porosity, and surface chemistry, *etc.*) influence H_2O_2 activation.[1,4,20–23]

This paper mainly focus on analyzing the relationships between morphological and chemical features of biochars (produced from different charring temperatures and modifications) and their performance in the activation of H_2O_2, in order

[a]*College of Environmental Science and Engineering, Hunan University, Changsha, Hunan 410082, P. R. China. E-mail: huangdanlian@hnu.edu.cn; Fax: +86 731 88823987; Tel: +86 731 88823987*

[b]*Key Laboratory of Environmental Biology and Pollution Control, Hunan University, Ministry of Education, Changsha, Hunan 410082, P. R. China*

to design improved chars. Considering the negative effects on ecosystem and human health from sulfamethazine (SMT) and the established mechanism of SMT degradation by $^{\cdot}OH$, SMT was selected as the target contaminant to evaluate the degradation efficiency of organic contaminants by H_2O_2/biochar system.[24–27]

2. Materials and methods

2.1. Chemicals

Sulfamethazine was obtained from Sigma Chemical Company (99%, w/w). Hydrogen peroxide (H_2O_2, 30%), titanium(IV) oxysulphate (15 wt% in dilute sulphuric acid, 99.99%), salicylic acid (99.5%), 2,3-dihydroxybenzoic acid (2,3-DHBA, 99.8%), and 2,5-dihydroxybenzoic acid (2,5-DHBA, 99.8%) were purchased from J&K Scientific Ltd, China. The rest of the chemicals was purchased from China National Medicines Corporation Ltd (Beijing, China), ultra-pure water (resistivity of 18.2 MΩ cm) was used throughout the experiments. Wheat straws were used in this study, which were collected from a village of Changsha (N27.9179, E113.199), Hunan province, China. It contained approximately 36.9% cellulose, 23.6% hemicellulose and 9.2% lignin according to previous methods.[28–30]

2.2. Biochar preparation

Wheat straws were rinsed with ultra-pure water four times and dried overnight, then oven-dried biomass was crushed and screened into 60 mesh. For pyrolysis, the resulting biomass was pyrolyzed with N_2 purge (0.5 L min^{-1}) at 10 °C min^{-1} in a tube furnace. The treated samples were kept at the target temperature between 300 and 800 °C for 2 h. After allowing the char to cool to room temperature, the char was placed in an air-tight container and stored in the dark before use. The chars were designated as W300, W400, W500, W600, W700, and W800, consisted with the pyrolysis temperature, respectively.

2.3. Oxygenation of biochar surface

100 mg of biochar sample W800 was added into 100 mL of 16% HNO_3 and agitated at 160 rpm at 80 °C for 3 h. The resulting sample was rinsed with ultra-pure water until constant pH, and dried in a vacuum drying oven. Then the oxygenated biochar, which retained the original textural properties and obtained the higher amount of surface functionalities, was available for further study.

2.4. Removal of inorganics

100 mg of biochar samples (W300, W500, and W700) were immersed in 100 mL of 16% HCl at 160 rpm at 25 °C for 24 h, the resulting samples were rinsed with ultra-pure water until constant pH, and dried in a vacuum drying oven, resulting in the deashed biochar, which had been removed all of inorganics.

2.5. Generation of $^{\cdot}OH$ in H_2O_2/biochar system

A series of experiments were performed in 100 mL conical flasks consisting of 50 mL of reaction solution. First, 50 mg of biochars was hydrated in 48 mL phosphate buffer solution (PBS, 10 mM, pH 7.4), at 25 °C for 10 min. Subsequently, 1.0 mL salicylic acid (SA, the final concentration was 2.0 mM), 1.0 mL H_2O_2 (the final concentration was 10 mM) were quickly added in sequence to initiate reaction. Then the flasks were in an incubator shaker with a shaking rate of 160 rpm at 25 °C for 2 h in the dark. Periodically, the suspension was filtered with 0.22 μm membranes glass microfiber filters for further analysis, and 1.0 mL ethanol was immediately added into 4.0 mL solution to quench the reaction. All of the experiments were performed in triplicate. Blank experiments without biochar or H_2O_2 were carried out under identical reaction conditions.

2.6. Degradation of SMT in H_2O_2/biochar system

To evaluate the broad application prospect of H_2O_2/biochar system on contaminants removal, the degradation efficiency of SMT in this system was studied. Batch experiments were carried out following the procedure described in Section 2.5, except SMT (the final concentration was 13.7 mM) was added instead of SA. Control experiments were performed under identical reaction conditions in the absence of H_2O_2 or biochar. In this study, the degradation efficiency of SMT was calculated based upon the values of SMT concentrations in "aqueous" and "solid" phases. To quantify the concentration of SMT in "solid" phases, the reacted chars were filtered and extracted by hexyl hydride, and the recovery ratio of SMT was 93–105%.

2.7. Characterization methods

Elemental (C, H, N and O) compositions of each char sample were determined using an elemental analyzer (model EA1110, CE Instruments, Milan, Italy). The extractable metals (Ca, Mg, Fe, Zn, and Mn) were determined by Atomic Absorption Spectrometry (Z-2000, Hitachi, Japan) following the acid digestion, the content of K was determined using Flame Photometry (FP640, Inesa, China).[11,31]

Surface area (S_{BET}) and pore volume were determined by N_2 adsorption at 77 K and CO_2 adsorption at 273 K with a surface area analyzer after outgassing at 473 K (ASAP-2020, Micromeritics Instrument Corporation, USA).[32,33] The morphologies of biochars were characterized by environmental scanning electron microscopy (ESEM) (JSM-5600, Japan) at an accelerating voltage of 20 kV. X-ray photoelectron spectroscopy (XPS) was obtained with a Thermo ESCALAB 250XI system with Al Kα radiation at 1486.6 eV.

The pH of biochar samples was measured by combining biochar with ultra-pure water at the ratio of 1 : 20 (w/v) after being stirred at 160 rpm at 25 °C for 2 h (FE20K, Mettler Toledo, USA). The surface acidity and basicity of chars were determined by "base adsorption" and "acid adsorption", respectively.[34,35] The base or acid uptake of biochar was converted to the content of surface acidity or surface basicity (cmol kg^{-1}), respectively. Moisture, volatile matter (VM), fixed carbon, and ash contents of these chars were measured according to the American Society for Testing and Materials (ASTM) D5124.[36]

2.8. Analysis methods

The concentrations of hydroxyl radicals were indirectly measured following a salicylic acid (SA) method.[11] SA can react with ˙OH, which would cause for the formation of 2,3-dihydroxybenzoic (2,3-DHBA), 2,5-dihydroxybenzoic (2,5-DHBA) and catechol.[37] High performance liquid chromatography (HPLC) (Series 1100, Agilent, Germany) equipped with a Zorbax SB-C18 column (4.6 × 250 mm, 5 μm, Waters) was applied to the analysis of SA, 2,3-DHBA and 2,5-DHBA. Details about the analysis and calculation method were reported by Fang *et al.*[11]

Details about the measurement of SMT were described in our previous study.[25] The concentrations of H_2O_2 were analyzed by UV-vis spectrophotometer (2700, Shimadzu Corporation, Japan) following a colorimetric method.[38]

3. Results and discussion

3.1. Characteristics of the biochars

With the increasing of heat treatment temperatures (HTT), O and H content decreased whereas C content increased, leading to the reductions in H/C, O/C molar ratios of these samples (Table 1, Fig. 1). H/C and O/C molar ratios have been analyzed to evaluate the degree of aromaticity and polarity of chars, respectively.[39] The decrease of H/C value was closely correlated to the stronger carbonization of biochar, which indicated that high carbonizing temperature may result in the formation of higher aromatic ring structures in biochars.[22,40] The reduction of O/C value with increasing pyrolysis temperature may cause biochars to be less hydrophilic. In addition, the molar ratio of (O + N)/C of the samples, as a polarity index indicator, decreased with elevation of pyrolysis temperature, which indicated a reduction of the surface polar functional groups. The results of the XPS C1s peaks were presented in Fig. 2, which clearly showed the formation and variation of oxygen-containing functionalities of biochars. The photoelectron peak was resolved into four curves with peaks of approximately 284.8, 286.2, 289.8, 290.5 eV, which represented aliphatic/aromatic carbon (C–C, C–H, and C=C), C–O, O–C=O, and carbonate groups,[25] respectively. In Table 2, aliphatic/aromatic carbon and carbonate groups might developed whereas C–O decreased as the increase of HTT, and carbonate groups would be strong after 600 °C.

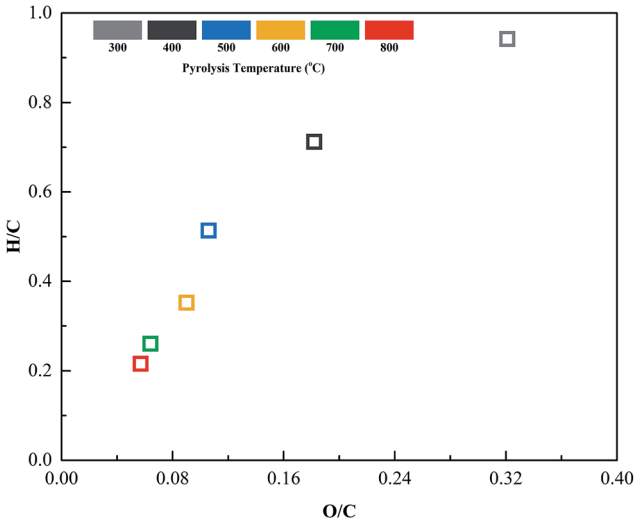

Fig. 1 The van Krevelen plot of elemental ratios for biochars formed from a series of HTT.

Table 1 Proximate and ultimate analyses of biochars produced at a series of HTT

Characteristics	W300	W400	W500	W600	W700	W800
Proximate analysis[a]						
pH	6.92 ± 0.02	7.34 ± 0.04	7.69 ± 0.01	8.13 ± 0.05	8.42 ± 0.03	8.53 ± 0.04
Yield (%)	52.31 ± 0.66	38.88 ± 0.22	35.52 ± 0.45	31.12 ± 0.28	29.72 ± 0.21	28.42 ± 0.32
Ash (%)	7.10 ± 0.23	11.29 ± 0.17	12.42 ± 0.11	14.24 ± 0.22	14.92 ± 0.12	15.29 ± 0.28
VM (%)	58.49 ± 0.42	32.72 ± 0.31	20.81 ± 0.16	14.59 ± 0.18	11.37 ± 0.31	9.78 ± 0.14
Fixed C (%)	31.18 ± 0.44	52.11 ± 0.14	61.68 ± 0.22	65.15 ± 0.34	67.90 ± 0.14	68.72 ± 0.42
Moisture (%)	3.23 ± 0.03	3.88 ± 0.01	5.09 ± 0.05	6.02 ± 0.08	5.81 ± 0.02	6.21 ± 0.04
Ultimate analysis						
C[b] (%)	65.2	75.5	82.9	85.5	88.8	89.9
H[b] (%)	5.12	4.48	3.55	2.51	1.93	1.62
O[b] (%)	27.92	18.29	11.75	10.28	7.59	6.83
N[b] (%)	1.76	1.73	1.80	1.71	1.68	1.65
Molar H/C	0.942	0.712	0.514	0.352	0.261	0.216
Molar O/C	0.321	0.182	0.106	0.09	0.064	0.057
Molar (O + N)/C	0.344	0.201	0.125	0.107	0.08	0.073
K (g kg^{-1})	12.43	16.74	15.5	15.78	15.64	15.66
Ca (g kg^{-1})	15.45	19.15	20.7	20.37	20.64	19.85
Mg (g kg^{-1})	2.12	3.15	2.84	2.83	2.54	2.57
Fe (g kg^{-1})	1.52	1.43	1.36	1.31	1.25	1.23
Mn (g kg^{-1})	0.11	0.14	0.13	0.12	0.11	0.12
Total (wt%)	3.16	4.06	4.05	4.04	4.01	3.94

[a] Mean ± standard deviation (SD) in triplicate measurements. [b] Elemental compositions and atomic ratios are on an dry ash-free basis.

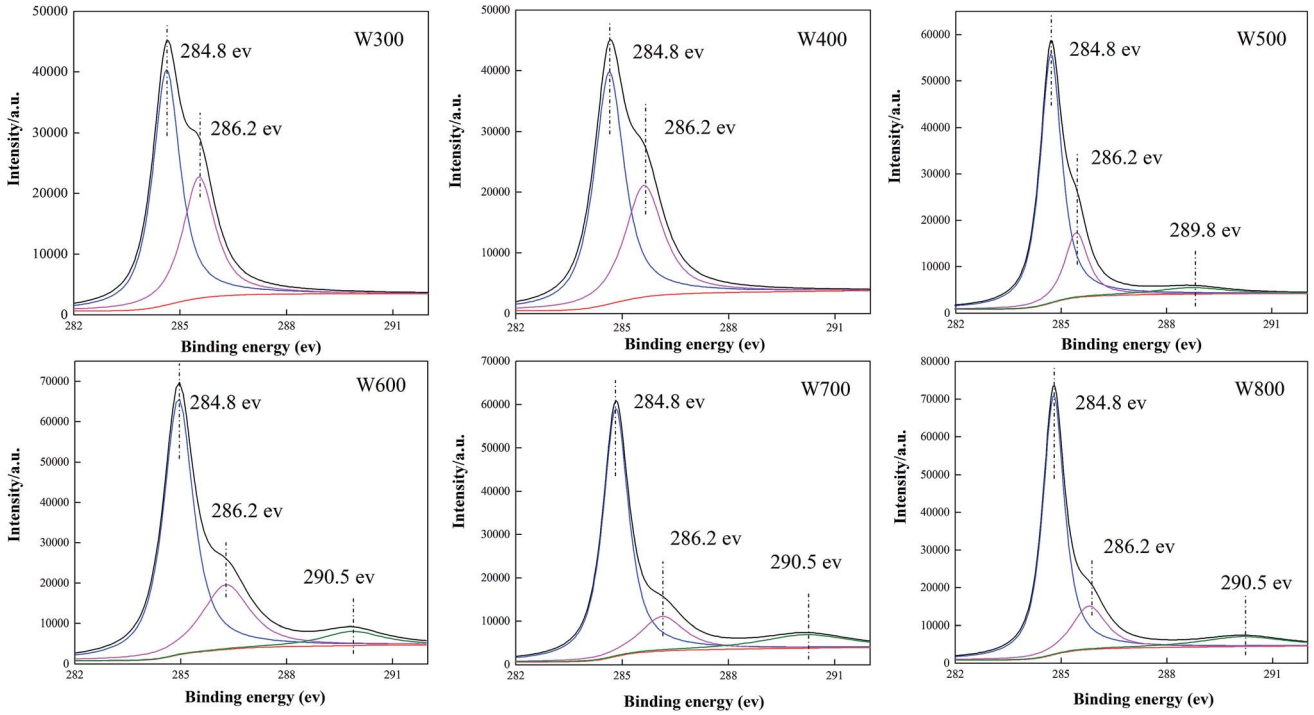

Fig. 2 Deconvolution of XPS C1s for biochars formed from a series of HTT.

The variations of extractable constitutes (K, Ca, Mg, Fe and Mn) with the increasing charring temperature were presented in Table 1. It was clear that extractable cations obviously changed from 300 °C to 500 °C and trended towards stability for subsequent temperature. As shown in Fig. 3, the acidity of biochars was thought to be the amount and strength of being acid, such as carboxyl, lactone, phenol, *etc.* The surface alkalinity of biochars was determined by the quality or state of basic sites: (1) some of oxygen functional groups, (2) heteroatom (except oxygen) functional groups, (3) inorganic matters, (4) π-electrons and edge-electron pairs (Fig. 3).[41] The surface acidity decreased whereas the surface alkalinity increased with increasing pyrolysis temperature (Table 3), which was consistent with the result of XPS. The trend of pH with increasing HTT was consistent with that of ash content, resulting from the development and migration of the alkalinity and carbonate content.

The changes in VM and fixed carbon contents occurred mostly at 300–500 °C due to the decomposition of biopolymer including hemicellulose, cellulose, and lignin (Table 1). Given that VM was relative to contents of the labile fraction of biochar, the rapid decline of VM may indicate that the higher temperature led to the higher stabilization.[42] The textural characteristics of the biochars were closely related to the pyrolysis temperature, and the results were given in (Table 3, Fig. 4). The extremely low value in S_{BET} (8.9 m^2 g^{-1}) and porosity (0.006 cm^3 g^{-1}) of W300 suggested that the decomposition of biopolymers was not marked at relatively low HTT. With increasing charring temperature, the formation and release of volatile organic components significantly intensified the development of pore nature and surface area. The results showed that the surface area and porosity of the samples both improved rapidly from 8.9 (W300) to 223.4 (W800) m^2 g^{-1}, and 0.006 (W300) to 0.105 (W800) cm^3 g^{-1}, respectively.

The effects of these characteristics on H_2O_2 activation in H_2O_2/biochar system would be later discussed in Section 3.3.

3.2. Generation of ˙OH in H_2O_2/biochar system

To verify the hypothesis that the morphological and chemical features of biochar affect the H_2O_2 activation, biochars

Table 2 C1s bonding state and its relative atomic percentage on the biochar samples

		Peak concentration (%)					
Peak (eV)	Assessment	W300	W400	W500	W600	W700	W800
284.8	C–C, C–H, or C=C	61.97	63.31	65.90	73.14	73.43	74.20
286.2	C–OH, C–O–C	38.03	36.69	26.68	20.51	17.11	16.32
289.8	COOH, COOC	N/D[a]	N/D	7.42	N/D	N/D	N/D
290.5	Carbonate groups				6.35	9.46	9.48

[a] XPS analysis showed no presence due to the extremely low content.

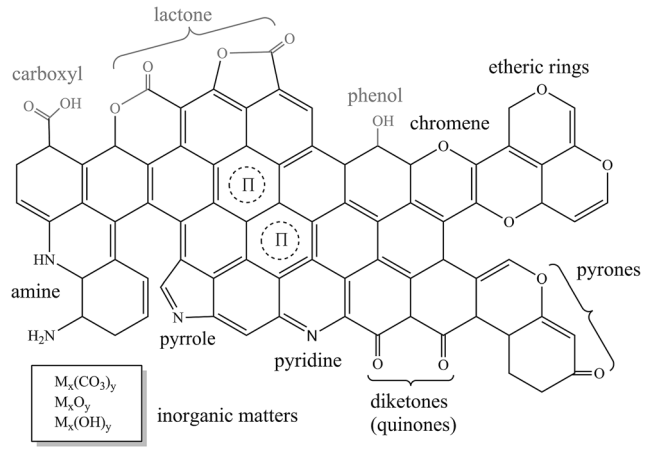

Fig. 3 An overview of acidic sites (light grey) and basic sites on the surface of biochars.

(pyrolyzed at a series of HTT) were utilized as catalyst, the corresponding values in H_2O_2 decomposition and $^{\cdot}OH$ yields were measured in this study. SA, a chemical probe of $^{\cdot}OH$, was used to measure the concentrations of $^{\cdot}OH$ radicals generated in H_2O_2/biochar system. In this part, the rate of H_2O_2 decomposition was described as eqn (1),

$$[H_2O_2] = [H_2O_2]_0 e^{-k_d t} \quad (1)$$

where k_d is the pseudo-first-order rate constant, $[H_2O_2]_0$ is the initial concentration of H_2O_2, and $[H_2O_2]$ is the concentration at reaction time t. Thus k_d can be determined by linear regression of plot of $\ln([H_2O_2]/[H_2O_2]_0)$ against t. Fig. 5(a) revealed that both the decomposition of H_2O_2 and the corresponding pseudo-first-order rate constants (k_d) increased with the increasing HTT. As shown in Fig. 5(b), trapped [OH] increased linearly from 6 to 98 μM for W300, 8 to 112 μM for W400, 11 to 164 μM for W500, 12 to 202 μM for W600, 15 to 234 μM for W700, and 14 to 255 μM for W800 during reaction time of 2 h, respectively. The results indicated that chars produced at higher HTT had higher capacity in promoting the decomposition of H_2O_2 and the formation of $^{\cdot}OH$.

It has been reported that the morphological and chemical features of biochar were significantly impacted by the pyrolysis temperature,[21–23] and the H_2O_2 activation was initiated on the surface of the biochar, the differences in above-mentioned results might result from the differences in surface area, porous structure, and surface chemistry. Therefore, the influences of those properties in H_2O_2 activation were further investigated and discussed in the following section.

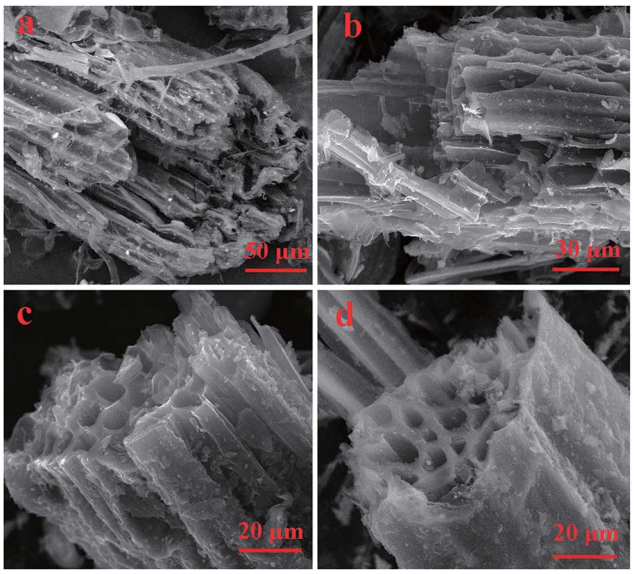

Fig. 4 ESEM images of biochars produced through pyrolysis at 300 °C (a), 500 °C (b), 700 °C (c) and 800 °C (d).

3.3. Influence of morphological and chemical features

3.3.1. Influence of the morphological properties on H_2O_2 activation. The relationships between the concentrations of trapped [OH] and S_{BET}/porosity of biochars were investigated to insight how the surface structural and porosity influence the formation of $^{\cdot}OH$. The yields of trapped [OH] increased proportionately with increasing S_{BET} or expanding porosity (Fig. 6(a) and (b)), and the corresponding correlation coefficient was 0.975 for S_{BET}, and 0.967 for porosity, respectively. The strong positive correlations indicated that the surface availability and the porosity were important factors in controlling $^{\cdot}OH$ generation in the system. According to Rey *et al.*,[43] free radicals species might be generated from H_2O_2 activation by activated carbon, and the mechanism could be explained by an electro-transfer reaction. In the process of the electron transfer, the biochar acted as both an adsorbent and a catalyst, in which case its textural properties (surface area/microporous) may plan an important role. On the one hand, well development of surface area may provide a convenience for the presence of the considerable unsaturated carbons atoms and functional groups, resulting in high concentration of unpaired electrons and active sites. On the other hand, the higher surface area meant more opportunities for H_2O_2 molecules to be able to interact with active sites of biochars. Concerning that the

Table 3 Values of S_{BET}, pore volume, surface acidity, and surface basicity for biochars produced at a series of HTT

Characteristics	W300	W400	W500	W600	W700	W800
S_{BET} ($m^2\ g^{-1}$)	8.9	22.9	108.1	185.4	216.3	223.4
Pore volume ($cm^3\ g^{-1}$)	0.006	0.018	0.058	0.089	0.095	0.105
Surface acidity[a] (cmol kg^{-1})	183.4 ± 3.6	130.2 ± 2.8	86.4 ± 3.1	60.4 ± 2.3	54.3 ± 1.3	48.9 ± 3.4
Surface basicity[a] (cmol kg^{-1})	84.9 ± 2.9	108.4 ± 4.3	128.7 ± 5.1	139.7 ± 3.1	143.6 ± 3.9	146.2 ± 4.8

[a] Mean ± standard deviation (SD) in triplicate measurements.

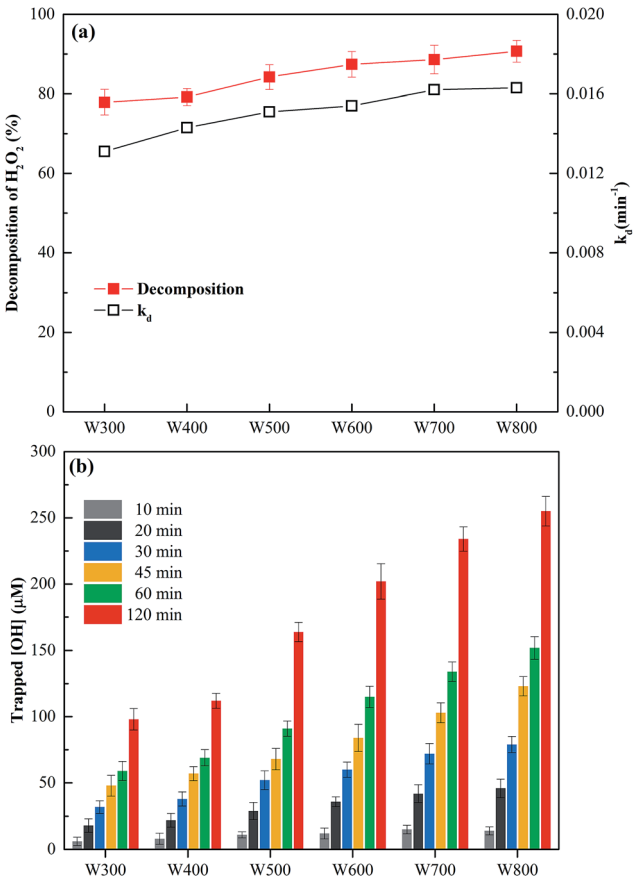

Fig. 5 Activation of H_2O_2 with a series of biochars produced at different HTT. Decomposition of H_2O_2 in H_2O_2/biochar system (a). Changes of trapped [OH] concentrations in H_2O_2/biochar system quantified by SA method (b). Reaction conditions: reaction time = 2 h; [biochar] = 1.0 g L^{-1}; [H_2O_2] = 10 mM; [salicylic acid] = 2.0 mM; T = 25 °C; pH = 7.4 (10 mM PBS).

catalyst capacity of biochars might depend on the shifting of electron density, the greater microporous texture enhanced this process by creating a crosslinked network for electron transfer.

3.3.2. Influence of surface chemistry on H_2O_2 activation. It's well known the surface functional groups, especially basic groups, can be identified by carbonizing on the surface of biochars under an inert condition.[9,42] The fact, the functional groups and condensed aromatic sheets were positive correlated with the redox properties of chars, which has been reported in the literature.[15] Similarly, Ribeiro *et al.*[38] has reported that the catalytic activity of activated carbon was closely linked with surface chemistry, and less oxygen-containing functionalities meant higher catalytic activity. The effects of surface functionalities were analyzed by determining the trapped [OH] concentrations from the H_2O_2 decomposition reaction by biochar.

Table 3 revealed that surface acidity decreased while surface alkalinity increased with the increasing pyrolysis temperature. The results showed that the relatively higher temperature enhanced the removal of acidic active sites and promoted the formation of basic active sites, which made access to a great basic character for biochar (development of pH value). As presented in Fig. 6(c) and (d), the changes of surface acidity and basicity of chars were closely connected to the formation of ˙OH. Obviously, there was a negative correlation between the concentrations of trapped [OH] and surface acidity (Fig. 6(c), R^2 = 0.843), while a positive correlation for surface basicity (Fig. 6(d), R^2 = 0.863). Similarly, several papers has reported that carbon materials with great surface basicity has more activity for H_2O_2 decomposition.[44,45] According to Ribeiro *et al.*,[38] the increasing basicity of carbon materials promoted ˙OH formation from H_2O_2 decomposition.

As shown in Fig. 7(a) and (b), it was seen that the modified biochars showed lower capacity, which had more acid oxygen-containing functionalities and higher values of surface acidity. The preparation for the modified sample was described in Section 2.3. The sample char W800 was selected, because of the minimum of the acid oxygen-functionalities and stabilized textural properties. Compared with the original biochar, the oxygenated biochar had 8% and 5% decrease in surface area and total pore volume, respectively. Acidity increased from 48.9 to 97.6 cmol kg^{-1}, and basicity decreased from 146.2 to 105.7 cmol kg^{-1}. This suggested that acid oxygen-functionalities had been successfully inserted onto the surface. The reactivity of the original biochar was compared to that of the oxygenated biochar, which had similar textural properties but more acid oxygen-functionalities on the surface. The results in Fig. 7(a) and (b), showed that remarkably difference between the original biochar and the oxygenated biochar in the H_2O_2 activation and ˙OH formation. It can be concluded that the oxygenated biochar had lower catalytic activity for H_2O_2 activation and the formation of ˙OH than original biochar.

Summarizing, the H_2O_2 decomposition rate may increase in the presence of strong basic functionalities and weak acid oxygen-functionalities on the biochar surface. Considering the acid oxygen-functionalities had an electron withdrawing capacity,[9,45] the process of the electron transfer would be inhibited and led to the decrease of ˙OH formation in H_2O_2/biochar system. On the contrary, basic functionalities acting as proton sinks would exhibit a strong positive charge on the surface of biochar, improving the electron transfer effects.[38,41,46] Thus, these functional groups could be recognized as active sites for H_2O_2 decomposition and contributed to enhance the generation of ˙OH radicals.

3.3.3. Influence of inorganics on H_2O_2 activation. The agglomeration of inorganics has been observed on the surface of chars and reported by Helsen and Hacala.[47] The agglomeration of inorganics on the biochar surface was supported in ESEM (Fig. 4). The state of inorganics on the char surface developed and changed with the increase of HTT, which resulted from the migration and agglomeration of both oxygen and metals onto the biochar surface. As shown in Table 1, biochar samples contained metals in its composition (approximately 4%).

A new research demonstrated that inorganics (Ca, K, Na, Si, P, and Mg) were observed in the poplar wood biochar, and biochar with higher contents of inorganics had higher catalytic performance in methane-cracking reactions.[48] Fang *et al.*[12] noted that changing in the types and concentrations of metals may significantly alter the ability to activate persulfate of

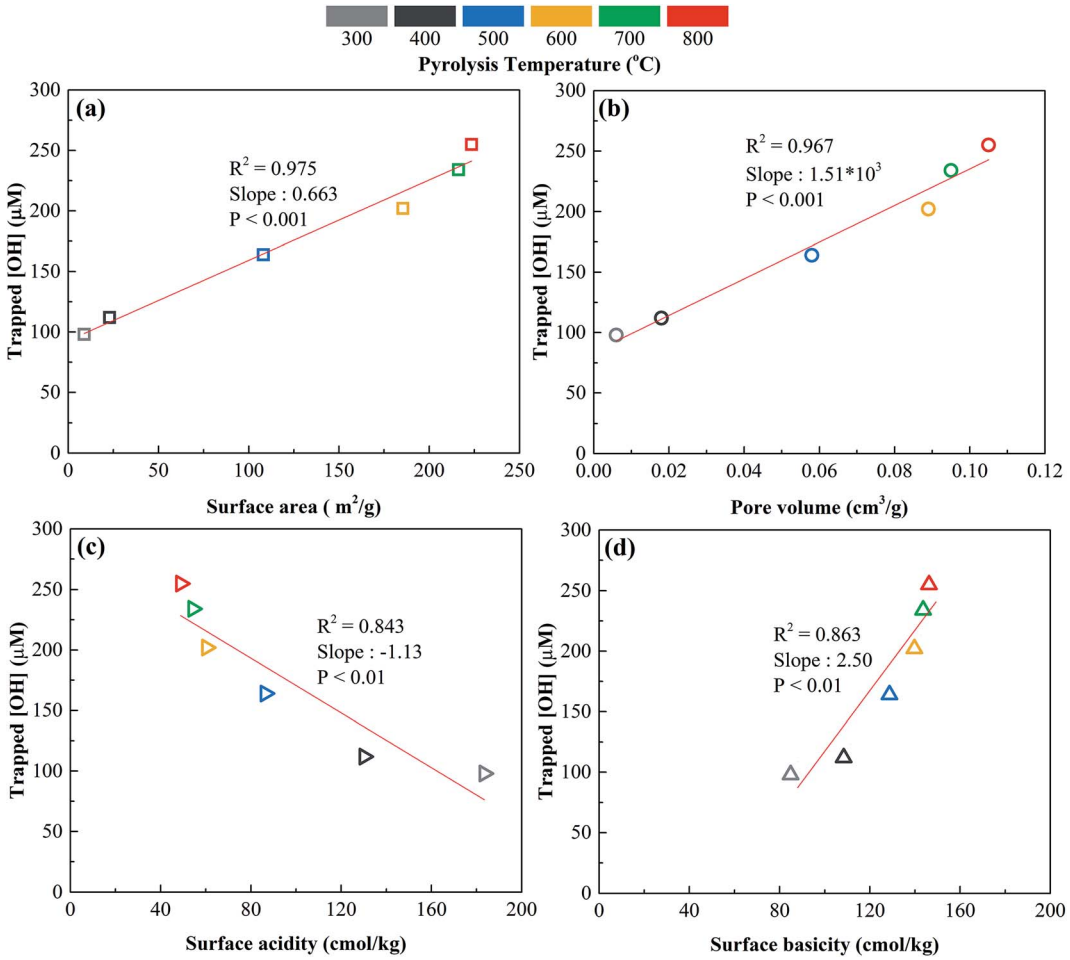

Fig. 6 Correlations between the concentrations of trapped [OH] and the structural and surface properties of biochars in surface area (a), pore volume (b), surface acidity (c), surface basicity (d).

biochar. Therefore, we investigated that whether inorganics played an important role in activating H_2O_2. The deashed chars, which produced from the procedure described in Section 2.4 and removed more than 95% of inorganic fractions, were compared to the original char samples by measuring the yields of the trapped $^{\cdot}OH$. As presented in Fig. 7(c), the trapped $^{\cdot}OH$ concentrations decrease 18%, 23%, 24% compared to that of the original char samples, W300, W500, and W700, respectively. These results suggested that the inorganic matters, which only made up approximately 4% (w/w) of biochars, surely did a considerable contribution to the generation of $^{\cdot}OH$ radicals from the H_2O_2/biochar system. Additionally, this also indicated that the deashed biochars had catalytic activity. As a result, the presence of the surface area/porous texture, which had no loss in the acid treatment, played an important role in the process that the biochar activates H_2O_2.

Given that the importance of inorganics in H_2O_2 activation of char was remarkable, we explored whether ash, made up of only inorganics, would exhibit a better performance in activating H_2O_2 than that of char. W800 was heated in an open crucible to 800 °C for 45 min to produce the ash. Compared with the original char sample, this production lost more than 99% of the organic fractions (carbon) and was made up of the metals and minerals. The experiments were carried out according to the procedure described in Section 2.5. The ash exhibited relatively poor performance in activating H_2O_2 than the char, as demonstrated by the low yields of trapped [OH] in Fig. 7(a), indicating that the presence of organic carbon was essential to the generation of $^{\cdot}OH$ radicals in the H_2O_2/biochar system. Some possible explanations could be proposed for these: (1) interactions between organic and inorganic fractions may contribute to the process that the char activates H_2O_2; (2) carbon can be considered as supports, on which inorganics are dispersed randomly, associated with their excellent surface nature; (3) some active sites adhered closely to the surface on organic carbon were linked with the H_2O_2 decomposition.

3.4. Degradation kinetics of SMT

To evaluate the removal efficiency of organic pollutants in H_2O_2/biochar system, the experiments for SMT degradation were carried out following the procedure described in Section 2.6. Fig. 8 showed that the degradation efficiency of 13.7 μM SMT was 93.2% for W300/H_2O_2, 100% for W500/H_2O_2, and 100% for W700/H_2O_2, respectively, during reaction time of 2 h.

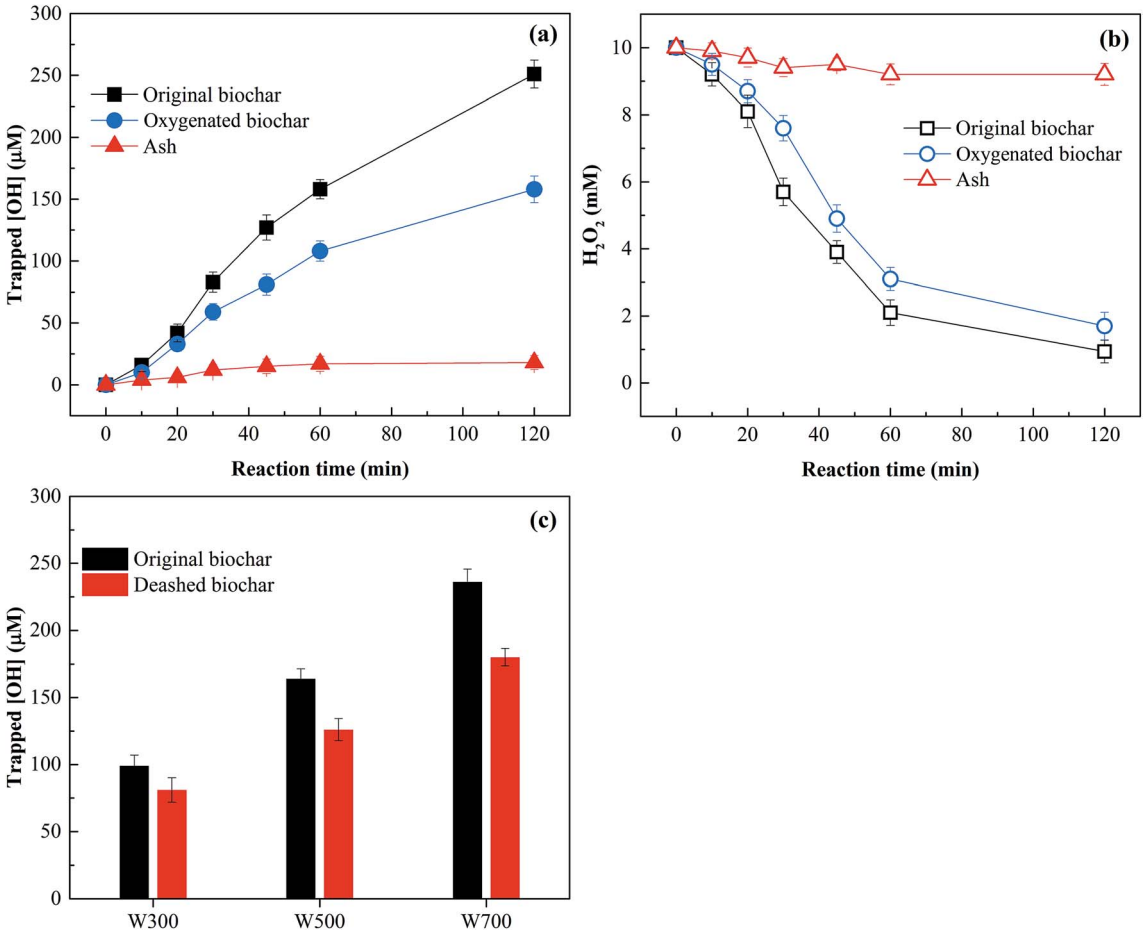

Fig. 7 Comparisons between original biochar and modified biochars/ash. (a) Comparisons between original biochar and oxygenated biochar or ash on the formation of ˙OH radicals. (b) Comparisons between original biochar and oxygenated biochar or ash on decomposition of H_2O_2. (c) Comparison between original biochar and deashed biochar on the formation of ˙OH radicals. Reaction conditions: [biochar] = 1.0 g L^{-1}; [H_2O_2] = 10 mM; [salicylic acid] = 2.0 mM; T = 25 °C; pH = 7.4 (10 mM PBS).

Oppositely, only 6.3%, 8.6%, 9.3% of SMT was removed in the system without H_2O_2, which was mostly depended on the adsorption on char under the identical reaction conditions. Additionally, less than 5% of SMT disappeared in control experiments without biochar. The degradation of SMT can be described by following equation (eqn (2)),

$$[\mathrm{SMT}] = [\mathrm{SMT}]_0 e^{-k_{obs}t} \quad (2)$$

where k_{obs} is the pseudo-first-order rate constant, $[\mathrm{SMT}]_0$ is the initial concentration, and [SMT] is the concentration at reaction time t. Thus k_{obs} can be determined by linear regression of plot of $\ln([\mathrm{SMT}]/[\mathrm{SMT}]_0)$ against t. As shown in Table 4, k_{obs} for SMT degradation increased with the increasing of HTT in H_2O_2/biochar system. These results suggested that H_2O_2/biochar system had a broad application prospect on SMT degradation, and the higher HTT, the higher efficiency. Furthermore, ethanol, a scavenger of ˙OH, was used to identify that ˙OH radicals were primarily attributed for SMT degradation in H_2O_2/biochar system. As shown in Fig. 8, with the addition of 10.0 mM ethanol, the degradation efficiency of SMT plunged from

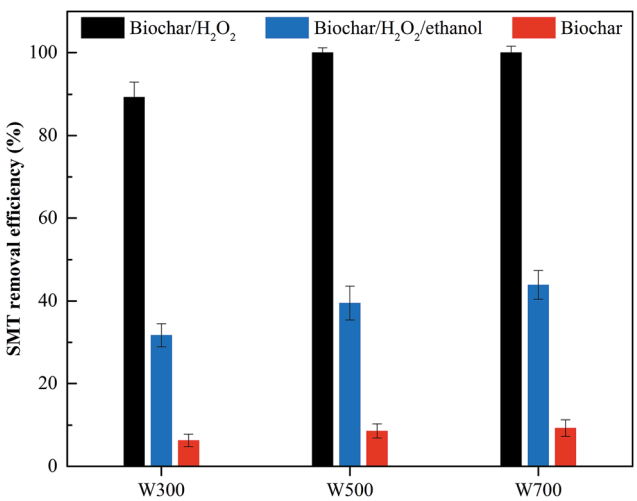

Fig. 8 Comparisons between H_2O_2/biochar and H_2O_2/biochar/ethanol or biochar only in SMT degradation. Reaction conditions: [biochar] = 1.0 g L^{-1}, [H_2O_2] = 10 mM, [SMT] = 13.7 μM, [ethanol] = 10 mM, T = 25 °C; pH = 7.4 (10 mM PBS).

Table 4 Values of the first-order rate constant for SMT degradation in H_2O_2/biochar system

Biochar	W300	W400	W500	W600	W700	W800
SMT degradation (%)	93.2	94.7	100	100	100	100
k_{obs} (min^{-1})	0.0211	0.0237	0.0324	0.0379	0.0411	0.0427
R^2	0.914	0.926	0.957	0.931	0.963	0.925

93.2% to 31.7% for W300, 100% to 39.5% for W500, 100% to 43.9% for W700, respectively. The results evidenced that well performance in SMT degradation was inseparable from the generation of ·OH in H_2O_2/biochar system.

According to several reports,[24,26,49–53] the ·OH radicals could attack the pyrimidine ring, aromatic ring or sulfonamide bond [N–S] of SMT molecule. The pyrimidine ring was broken by the cleavage of C=N bond and C–N bond, resulting in the formation of 4-amino-*N*-carbamimido-yl-benzenesulfonamide, formic acid (HCOOH), acetic acid (CH_3COOH).[26,49–51] The cleavage of sulfonamide bond [N–S], as the main pathway for SMT degradation, would lead to the formation of 4,6-dimethylpyrimidin-2-amine and sulfanilic acid.[24,26,49–52] Meanwhile, sulfate (SO_4^{2-}) could be released during this process. Sulfanilamide group could be oxidized to 4-aminophenol and then to 4-nitrophenol, which could be explained by the strong negative charge between aromatic ring and the nitrogen atom.[49–53] As the reaction progress, some of intermediates could be completely degraded to CO_2 and H_2O.[49–53] The possible pathways responsible for SMT degradation in this system could be proposed and described in Fig. 9.

Such the adsorption and degradation of SMT may be forced to coexist in this system. Thus how the surface adsorption of SMT would inhibit/accelerate the biochars' reactivity toward H_2O_2 and SMT degradation should be studied. For this purpose, the effects of adsorption time on biochar were investigated before using as a catalyst for H_2O_2 activation. As expected in Fig. 10(a) and (b), both the degradation of SMT and the decomposition of H_2O_2 were suffered markedly following the adsorption time extended, as demonstrated the visible decline in the pseudo-first-order rate constants of SMT degradation (k_{obs}) and H_2O_2 decomposition (k_d). The results were in agreement with Fang *et al.*,[11] which aimed at that of 2-chlorobiphenyl. The inhibition of H_2O_2 activation reactions might result from the variations in morphological and chemical features of biochar during the process of adsorption. More SMT

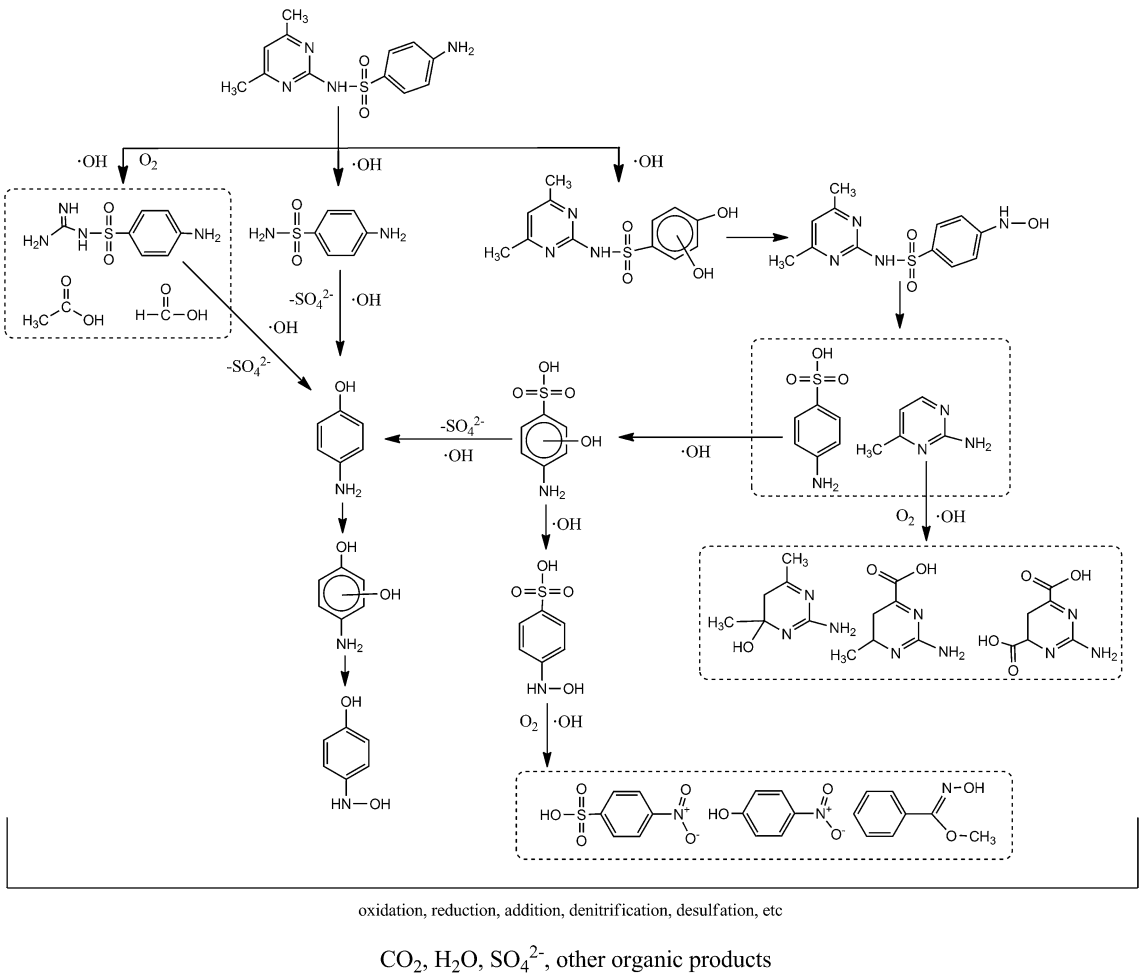

Fig. 9 Proposed pathways for SMT degradation in H_2O_2/biochar system.

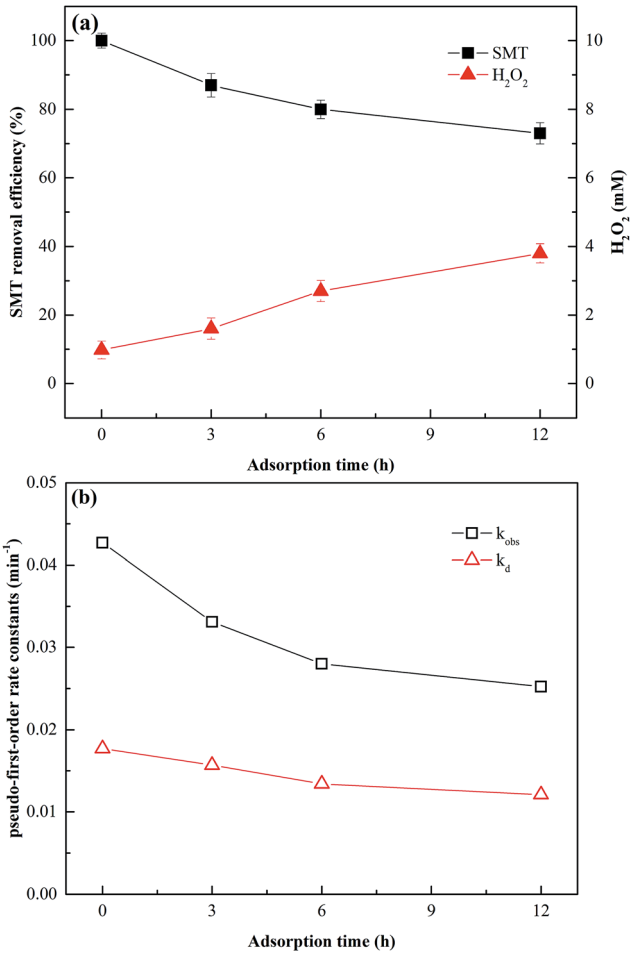

Fig. 10 Effects of SMT adsorption on H_2O_2 activation by W800. (a) Effects of adsorption time on SMT degradation and H_2O_2 decomposition in H_2O_2/W800 system. (b) k_d *vs.* adsorption time and k_{obs} *vs.* adsorption time. Reaction conditions: [biochar] = 1.0 g L^{-1}; [H_2O_2] = 10 mM; [SMT] = 13.7 μM; T = 25 °C; pH = 7.4 (10 mM PBS).

molecules adhered to surface and entered into the pore of biochar, which may cause the reduction of surface availability and the blocking of the pore. In our previous study,[25] π–π electron-donor–acceptor interaction and other physical-chemistry processes occurred on surface of chars during SMT adsorption, leading to the reduction in both electrons availability and active sites on the surface of biochar. Therefore, the accessibility of H_2O_2 was hindered as the adsorption time extended, the degradation of SMT was inhibited at the same time.

4. Conclusions

In this study, biochar exhibited favorable catalytic performance in H_2O_2 activation to generate $^{\cdot}OH$, promoting SMT degradation in aqueous solutions. There were linear relationships between the catalytic performance on H_2O_2 activation and morphological/chemical features of biochars, such as surface area (R^2 = 0.975), porosity (R^2 = 0.967), surface acidity (R^2 = 0.843), and surface basicity (R^2 = 0.863). Furthermore, the process that the biochar activates H_2O_2 was significantly hindered by the surface adsorption of SMT. Our findings provides a new approach for removal of organic contaminants, efficiently utilizing the performance of biochar as the catalyst in H_2O_2 activation.

Acknowledgements

This work was supported by the Program for the National Natural Science Foundation of China (51378190, 51278176, 51408206, 51579098, 51521006), the National Program for Support of Top-Notch Young Professionals of China (2014), the Fundamental Research Funds for the Central Universities, the Program for New Century Excellent Talents in University (NCET-13-0186), the Program for Changjiang Scholars and Innovative Research Team in University (IRT-13R17), Scientific Research Fund of Hunan Provincial Education Department (No. 521293050).

References

1 M. Ahmad, A. U. Rajapaksha, J. E. Lim, M. Zhang, N. Bolan, D. Mohan, M. Vithanage, S. S. Lee and Y. S. Ok, *Chemosphere*, 2014, **99**, 19–33.
2 J. Lehmann, J. Gaunt and M. Rondon, *Mitigation and Adaptation Strategies for Global Change*, 2006, **11**, 395–419.
3 E. Marris, *Nature*, 2006, **442**, 624–626.
4 X. Tan, Y. Liu, G. Zeng, X. Wang, X. Hu, Y. Gu and Z. Yang, *Chemosphere*, 2015, **125**, 70–85.
5 Y. Sun, B. Gao, Y. Yao, J. Fang, M. Zhang, Y. Zhou, H. Chen and L. Yang, *Chem. Eng. J.*, 2014, **240**, 574–578.
6 D. Kołodyńska, R. Wnętrzak, J. Leahy, M. Hayes, W. Kwapiński and Z. Hubicki, *Chem. Eng. J.*, 2012, **197**, 295–305.
7 S. G. Huling, E. Kan, C. Caldwell and S. Park, *J. Hazard. Mater.*, 2012, **205**, 55–62.
8 N. H. Ince and I. G. Apikyan, *Water Res.*, 2000, **34**, 4169–4176.
9 P. Serp and J. L. Figueiredo, *Carbon materials for catalysis*, Wiley Online Library, 2009.
10 S. G. Huling, P. K. Jones and T. R. Lee, *Environ. Sci. Technol.*, 2007, **41**, 4090–4096.
11 G. Fang, J. Gao, C. Liu, D. D. Dionysiou, Y. Wang and D. Zhou, *Environ. Sci. Technol.*, 2014, **48**, 1902–1910.
12 G. Fang, C. Liu, J. Gao, D. D. Dionysiou and D. Zhou, *Environ. Sci. Technol.*, 2015, **49**, 5645–5653.
13 J. Yan, L. Han, W. Gao, S. Xue and M. Chen, *Bioresour. Technol.*, 2015, **175**, 269–274.
14 A. Kappler, M. L. Wuestner, A. Ruecker, J. Harter, M. Halama and S. Behrens, *Environ. Sci. Technol. Lett.*, 2014, **1**, 339–344.
15 L. Klüpfel, M. Keiluweit, M. Kleber and M. Sander, *Environ. Sci. Technol.*, 2014, **48**, 5601–5611.
16 D. D. Dionysiou, M. T. Suidan, I. Baudin and J.-M. Laîné, *Appl. Catal., B*, 2004, **50**, 259–269.
17 J. A. Khan, X. He, N. S. Shah, H. M. Khan, E. Hapeshi, D. Fatta-Kassinos and D. D. Dionysiou, *Chem. Eng. J.*, 2014, **252**, 393–403.

18 T. M. El-Morsi, M. M. Emara, H. M. A. El Bary, A. S. Abd-El-Aziz and K. J. Friesen, *Chemosphere*, 2002, **47**, 343–348.
19 B. A. Smith, A. L. Teel and R. J. Watts, *Environ. Sci. Technol.*, 2004, **38**, 5465–5469.
20 K. Sun, K. Ro, M. Guo, J. Novak, H. Mashayekhi and B. Xing, *Bioresour. Technol.*, 2011, **102**, 5757–5763.
21 C. Lattao, X. Cao, J. Mao, K. Schmidt-Rohr and J. J. Pignatello, *Environ. Sci. Technol.*, 2014, **48**, 4790–4798.
22 M. Uchimiya, L. H. Wartelle, K. T. Klasson, C. A. Fortier and I. M. Lima, *J. Agric. Food Chem.*, 2011, **59**, 2501–2510.
23 M. Xie, W. Chen, Z. Xu, S. Zheng and D. Zhu, *Environ. Pollut.*, 2014, **186**, 187–194.
24 M. Pérez-Moya, M. Graells, G. Castells, J. Amigó, E. Ortega, G. Buhigas, L. M. Pérez and H. D. Mansilla, *Water Res.*, 2010, **44**, 2533–2540.
25 C. Zhang, C. Lai, G. Zeng, D. Huang, C. Yang, Y. Wang, Y. Zhou and M. Cheng, *Water Res.*, 2016, **95**, 103–112.
26 Y. Feng, J. Liu, D. Wu, Z. Zhou, Y. Deng, T. Zhang and K. Shih, *Chem. Eng. J.*, 2015, **280**, 514–524.
27 Y.-q. Gao, N.-y. Gao, Y. Deng, Y.-q. Yang and Y. Ma, *Chem. Eng. J.*, 2012, **195**, 248–253.
28 D.-L. Huang, G.-M. Zeng, C.-L. Feng, S. Hu, X.-Y. Jiang, L. Tang, F.-F. Su, Y. Zhang, W. Zeng and H.-L. Liu, *Environ. Sci. Technol.*, 2008, **42**, 4946–4951.
29 D.-L. Huang, G.-M. Zeng, C.-L. Feng, S. Hu, C. Lai, M.-H. Zhao, F.-F. Su, L. Tang and H.-L. Liu, *Bioresour. Technol.*, 2010, **101**, 4062–4067.
30 C. Zhang, L. Liu, G.-M. Zeng, D.-L. Huang, C. Lai, C. Huang, Z. Wei, N.-J. Li, P. Xu and M. Cheng, *Biochem. Eng. J.*, 2014, **91**, 149–156.
31 D. Wang, W. Zhang and D. Zhou, *Environ. Sci. Technol.*, 2013, **47**, 5154–5161.
32 M. Teixidó, J. J. Pignatello, J. L. Beltrán, M. Granados and J. Peccia, *Environ. Sci. Technol.*, 2011, **45**, 10020–10027.
33 D. Zhu, S. Kwon and J. J. Pignatello, *Environ. Sci. Technol.*, 2005, **39**, 3990–3998.
34 H. Boehm, *Carbon*, 1994, **32**, 759–769.
35 C.-H. Cheng and J. Lehmann, *Chemosphere*, 2009, **75**, 1021–1027.
36 A. Standard, *ASTM International*, West Conshohocken, PA, 2004.
37 Y. Li, T. Zhu, J. Zhao and B. Xu, *Environ. Sci. Technol.*, 2012, **46**, 10302–10309.
38 R. S. Ribeiro, A. M. Silva, J. L. Figueiredo, J. L. Faria and H. T. Gomes, *Carbon*, 2013, **62**, 97–108.
39 X. Zhao, W. Ouyang, F. Hao, C. Lin, F. Wang, S. Han and X. Geng, *Bioresour. Technol.*, 2013, **147**, 338–344.
40 W. Wu, M. Yang, Q. Feng, K. McGrouther, H. Wang, H. Lu and Y. Chen, *Biomass Bioenergy*, 2012, **47**, 268–276.
41 J. M. Tascón, *Novel carbon adsorbents*, Elsevier, 2012.
42 J. Lehmann and S. Joseph, *Biochar for environmental management: science, technology and implementation*, Routledge, 2015.
43 A. Rey, J. Zazo, J. Casas, A. Bahamonde and J. Rodriguez, *Appl. Catal., A*, 2011, **402**, 146–155.
44 R. S. Ribeiro, N. A. Fathy, A. A. Attia, A. M. Silva, J. L. Faria and H. T. Gomes, *Chem. Eng. J.*, 2012, **195**, 112–121.
45 V. P. Santos, M. F. Pereira, P. Faria and J. J. Órfão, *J. Hazard. Mater.*, 2009, **162**, 736–742.
46 R. S. Ribeiro, A. M. Silva, J. L. Figueiredo, J. L. Faria and H. T. Gomes, *Appl. Catal., B*, 2016, **402**(1), 146–155.
47 L. Helsen and A. Hacala, *J. Hazard. Mater.*, 2006, **137**, 1438–1452.
48 N. B. Klinghoffer, M. J. Castaldi and A. Nzihou, *Fuel*, 2015, **157**, 37–47.
49 Y. Liu, J. Hu and J. Wang, *Radiat. Phys. Chem.*, 2014, **96**, 81–87.
50 Y. Fan, Y. Ji, D. Kong, J. Lu and Q. Zhou, *J. Hazard. Mater.*, 2015, **300**, 39–47.
51 Y. Liu and J. Wang, *J. Hazard. Mater.*, 2013, **250**, 99–105.
52 A. G. Trovó, R. F. Nogueira, A. Agüera, A. R. Fernandez-Alba, C. Sirtori and S. Malato, *Water Res.*, 2009, **43**, 3922–3931.
53 Z. Guo, F. Zhou, Y. Zhao, C. Zhang, F. Liu, C. Bao and M. Lin, *Chem. Eng. J.*, 2012, **191**, 256–262.